



## OPEN ACCESS

## EDITED BY

Junjie Wang,  
Tsinghua University, China

## REVIEWED BY

Junbo Sun,  
University of Western Australia, Australia  
SALMABANU LUHAR,  
The University of Sheffield, United Kingdom

## \*CORRESPONDENCE

Ali Abbas,  
✉ ali.abbas@sydney.edu.au

RECEIVED 09 May 2024

ACCEPTED 10 September 2024

PUBLISHED 26 September 2024

## CITATION

Samrani P, Cao Y, Fimbres-Weihs G, Sanjaya E and Abbas A (2024) Effect of fly ash and ground waste glass as cement replacement in concrete 3D-Printing for sustainable construction. *Front. Built Environ.* 10:1430174. doi: 10.3389/fbuil.2024.1430174

## COPYRIGHT

© 2024 Samrani, Cao, Fimbres-Weihs, Sanjaya and Abbas. This is an open-access article distributed under the terms of the [Creative Commons Attribution License \(CC BY\)](#). The use, distribution or reproduction in other forums is permitted, provided the original author(s) and the copyright owner(s) are credited and that the original publication in this journal is cited, in accordance with accepted academic practice. No use, distribution or reproduction is permitted which does not comply with these terms.

# Effect of fly ash and ground waste glass as cement replacement in concrete 3D-Printing for sustainable construction

Phebe Samrani<sup>1</sup>, Yifang Cao<sup>2</sup>, Gustavo Fimbres-Weihs<sup>1</sup>, Eric Sanjaya<sup>1</sup> and Ali Abbas<sup>1\*</sup>

<sup>1</sup>School of Chemical and Biomolecular Engineering, The University of Sydney, Sydney, NSW, Australia, <sup>2</sup>School of Civil Engineering, The University of Sydney, Sydney, NSW, Australia

Concrete 3D printing is a promising manufacturing technology for producing geometrically complex structures efficiently and cost-effectively, by eliminating the need for formwork, reducing labor, and minimizing waste. This method has the potential to lower carbon emissions and resource use. However, it does not mitigate the carbon emissions associated with cement production. Nonetheless, utilizing waste materials in concrete 3D printing may reduce concrete carbon emissions and support recycling. This study investigates the use of two industrial waste materials—fly ash (FA) and ground waste glass (GWG)—as partial substitutes for ordinary Portland Cement (PC) in 3D printable cement paste. The chemical composition, particle size distribution, rheological properties, and flexural strength of the mixtures were analyzed. Results show that specimens containing waste materials achieved strengths comparable to traditional cement mixtures. The flexural strength reduction in 3D printed versus cast specimens varied across mixtures: control (66% reduction), FA20 (35%), FA10-GWG10 (35%), GWG10 (32%), FA10 (11%), and GWG20 (4%). Hence, incorporating waste materials in concrete 3D printing is recommended, as it maintains mechanical integrity while promoting recycling and upcycling of industrial waste.

## KEYWORDS

concrete 3D printing, fly ash, ground waste glass, sustainable construction, waste recycling

## 1 Introduction

The construction industry is a major contributor to global energy consumption and carbon emissions, responsible for 36% of energy usage and 40% of CO<sub>2</sub> emissions (Atradius, 2023). Cement production is particularly impactful, emitting approximately 900 kg of CO<sub>2</sub> per metric ton (Benhelal et al., 2013). Thus, improvements in sustainability and energy efficiency in the construction industry are crucial. The rising popularity of 3D concrete printing offers a way to streamline construction by cutting formwork time and enabling geometrically complex structures. It also offers potential for reducing energy-related emissions by up to 32% (Batikha et al., 2022). By integrating construction waste as Additive Materials (AM), 3D concrete printing can further mitigate emissions, address waste management challenges, and promote a circular economy, enhancing both cost-effectiveness and sustainability. Material costs, which constitute about 70% of 3D printing expenses, highlight the importance of

TABLE 1 Recent 3D printing studies involving waste materials.

Ref	Materials	Highlights
Panda et al. (2019)	Fly Ash (FA)	Up to 60% of FA mixed with PC, using nano-clay to replace chemical admixtures for improved durability
Rubio et al. (2017)	Silica fumes	Silica fumes (8 wt%) appear to improve mixture stability and reduce slump
Qian et al. (2021)	Furnace slag	Up to 70% slag used in 3D printing, achieved by neutralizing the alkaline environment with vinyl acetate and sodium ash
Muthukrishnan et al. (2020)	Rice husk	Explores the potential of agricultural waste in 3D printing and its associated shrinkage issues
Şahin et al. (2021)	Ground waste glass (GWG)	Demonstrates the superiority of printed concrete with recycled glass as aggregate and its ease of extrusion
Zhu et al. (2023)	Rubber Particle and polypropylene	Replaced sand between 0% and 100% volume to modify 3D printable sustainable cementitious composites and explored its associated strength requirement
Zun et al. (2021)	Waste glass	Shown mechanical, chemical, and hydrothermal activation for waste glass reinforced cement as sand replacement at 0, 10, 20, and 30%
Sun et al. (2021), Sun et al. (2023)	Copper fiber, solids	Studies electromagnetic and mechanical performance of 3D printed copper solids and fibers incorporated into cementitious composites to reduce EMW.
Singh et al. (2023)	Antimony tailings	Utilizes antimony tailings replacing sand that enhances durability and strength up to 100% replacement

incorporating waste materials to optimize both economic and environmental outcomes (Dey et al., 2022).

Bio-inspired architectures like the Bouligand structure (Moini et al., 2018) have been found to enhance fracture and damage tolerance, offering a unique load-displacement response without sacrificing strength, even in 3D printed forms compared with cast specimens. It is to our interest to combine the benefits of 3D printing and upcycling waste; which has been limited due to the challenges in meeting the contradictory rheological requirements necessary for effective 3D printing—high flowability during extrusion and sufficient shape retention post-extrusion to support layering (Roussel, 2018).

Cement substitutes in 3D concrete printing often include materials with pozzolanic properties (i.e., self-cementing), such as industrial by-products (fly ash, slag, silica fumes), demolition waste (concrete aggregates), and agricultural residues (rice husk) (Dey et al., 2022). Table 1 reviews various 3D printing studies that have incorporated waste materials. A study by Zhu et al. (2023) promoted sustainability development in the construction industry by incorporating rubber particles from waste tires and polypropylene fibers into 3D printable cementitious composites. The effect of different approaches for the activation of the alkali-silica reaction in concrete with waste glass were investigated (Sun et al., 2021b). Copper fibers and solids were incorporated in cementitious composites to enhance electromagnetic wave (EMW) absorption, which negatively impacts the human body, information, and equipment security (Sun et al., 2021a; Sun et al., 2023). Singh et al. (2023) utilized antimony tailings in fiber reinforced 3D printed concrete as an approach for sustainable construction materials. Hence, it is apparent that 3D printed concrete and cement composites incorporating waste offer innovative solutions while reducing waste and promote design flexibility in this research area. Beyond the use of waste materials, other techniques can be demonstrated for improving these processes, such as the use of electromagnetic waves (Sun et al., 2020) or using AI (Yao et al., 2023).

Fly ash (FA) from coal-fired power plants is a viable substitute for Portland Cement (PC) due to its abundance, particle shape, and composition (Aitcin, 2016), making it an attractive sustainable alternative rich in alumina and silica (Xia et al., 2019). Previous

research has examined the use of fly ash and waste glass in concrete (Ebrahimi et al., 2017; Bui Viet et al., 2020). For 3D printing, fly ash improves extrudability (Dey et al., 2022). Ground Waste Glass (GWG) is also utilized due to its ability to partially replace cement and act as filler, and for its low water absorption and high silica content (Yin et al., 2021). Studies have explored GWG as a supplementary cementitious material (SCM) (Bignozzi et al., 2015), in ultra-high-performance glass concrete (Tagnit-Hamou et al., 2016), and for adjusting rheology and mechanical properties (Du and Tan, 2014; Tagnit-Hamou et al., 2016; Yin et al., 2021). With their reactivity potential, FA and GWG are promising substitutes for cement in extrusion-based 3D printing, owing to their composition rich in SiO<sub>2</sub>, Ca, and Al (Nodehi and Taghvaei, 2021). Hence, GWG may be introduced into 3D printers as a binder or aggregate to improve the product strength, although this may complicate the extrusion process (Şahin et al., 2021).

To fully leverage the benefits of waste AM in 3D printing, it is crucial to develop a printable material palette that meets specific rheological requirements. Previous research has explored various material composition parameters, including the use of cement paste-based mixtures, the presence or absence of aggregates, and the ratios of aggregates to binder, water to binder, and chemical admixtures. Those studies aimed to assess their impact on the performance of extrusion-based 3D printing. Although AM can enhance extrudability, they may reduce buildability. To mitigate this, a combination of two or more waste-based chemical admixtures has been suggested to optimize both properties (Dey et al., 2022). Furthermore, the absence of a standardized framework for comparison complicates the interpretation of research outcomes, as these can vary widely depending on the specific configurations of individual 3D printer setups. Additionally, some research underscores the importance of process optimization in 3D printing, particularly during the initial stages (Reiter et al., 2018; Dey et al., 2022).

Given the complexity of matching the rheological properties to the requirements of 3D printing, this paper aims to investigate the application of FA and GWG as replacements for PC, selected for their abundance in the Australian market. This study examines two main factors: (1) the impact of their use on the extrusion rheology and (2) the mechanical performance of the printed mixes using the

TABLE 2 Mix designs for varying degrees of cement replacement.

Cement replacement (wt% of binder)			
Mix	Abbreviation	FA	GWG
1	Control	0	0
2	FA10	10	0
3	FA20	20	0
4	GWG10	0	10
5	GWG20	0	20
6	FA10-GWG10	10	10

Bouligand architecture of [Moini et al. \(2018\)](#), focusing particularly on their flexural strength.

## 2 Materials and methods

### 2.1 Raw materials

General Purpose Portland Cement (PC) was locally acquired (Dingo cement), whilst fine grade Fly Ash (FA) was provided by Delta Electricity, and recycled ground waste glass (GWG) was provided by IQ Renew. To meet the rheological property requirements for 3D printing, the following chemical admixtures were used in this study: high range water reducer admixture (HRWRA, Sika Viscocrete 10) and viscosity modifying admixture (VMA, Mastermatrix 362). For the GWG, the sample is already pre-grounded by the waste supplier and is utilized as-is.

### 2.2 Mixture preparation and mix design

The printed Bouligand structure follows the work of [Moini et al. \(2018\)](#), using the same printer setup. The Bouligand structure, characterized by its helicoidal fiber arrangement, imparts exceptional toughness, flexibility, and damage resistance, as seen in natural examples like crustacean exoskeletons and fish scales. This unique design is increasingly being mimicked in synthetic materials to create advanced composites for applications requiring high strength and resilience. ([Liu et al., 2022](#)). In this work, one “Bouligand” structure (with 90° pitch angle) was printed, and 6 blends were compared against a reference control mix that did not incorporate waste. The cast counterparts of each mixture were also of similar disc dimensions (50 mm in diameter, 8 mm height). The proportions for all the mixtures are detailed in [Table 2](#).

For each mixing batch, a total 125 g of binder, 1.5 mL of HRWRA, 2.8 mL VMA, and 60 mL of water were used. The mixing protocol was adapted from [Moini et al. \(2018\)](#). A Twister Venturi vacuum mixer was used to mix the ingredients. The chemical admixtures were first added and dispersed in water. This mixture was then mixed with the dry ingredients for 25 s at 200 rpm, followed by mixing for 90 s at 400 rpm 70% vacuum, and another 90 s at 400 rpm 100% vacuum. The water to binder ratio and the two chemical admixtures were kept constant for all mixtures.



FIGURE 1  
3D printer setup combining the stepper-motor driven extruder and Ultimaker 2+.

### 2.3 Extrusion-based 3D printer setup

3D printed cement composites were produced using a gantry based Ultimaker 2+ 3D printer combined with a stepper-motor driven extruder from Structur3D Discov3ry ([Figure 1](#)). As this printer is relatively small in scale, no fine or coarse aggregates were used in this study, only its cement components.

### 2.4 Material composition (XRF)

To determine the oxide composition of Portland cement, fly ash, and ground waste glass, a quantitative analysis is conducted using X-Ray Fluorescence (XRF). The oxides that contribute to the hydration process in cement chemistry are  $\text{SiO}_2$ ,  $\text{Al}_2\text{O}_3$ , and  $\text{Fe}_2\text{O}_3$ . Additionally, CaO contributes directly to the formation of calcium hydroxide or portlandite when dissolved in water. The XRF data is compiled in [Table 3](#) for reference.

The data show that PC contains a substantial amount of CaO (64%) and  $\text{SiO}_2$  (20%), which is expected. FA contains a significant amount of  $\text{SiO}_2$  (58%) and  $\text{Al}_2\text{O}_3$  (27%), while GWG has a high proportion of  $\text{SiO}_2$  (70%) and a smaller proportion of CaO (11%).

### 2.5 Particle size distribution

A Malvern Panalytical laser diffraction analyzer was used to measure the particle size with the assumption that particles are spherical in shape. [Figure 2](#) shows the particle size distributions for PC, FA, and GWG. [Table 4](#) summarizes the  $D_{10}$ ,  $D_{50}$ , and  $D_{90}$  values, which correspond to particle sizes for which 10 mass%, 50%, and 90% of the samples are respectively below this size. The value of  $D_{[4,3]}$  reflects the particle size that constitutes the bulk of the sample volume or mass

TABLE 3 Chemical compositions of PC, FA, and GWG from XRF measurement.

	SiO <sub>2</sub>	Al <sub>2</sub> O <sub>3</sub>	Fe <sub>2</sub> O <sub>3</sub>	CaO	TiO <sub>2</sub>	Na <sub>2</sub> O	K <sub>2</sub> O	MgO	Mn <sub>3</sub> O <sub>4</sub>	SO <sub>3</sub>	Loi
PC	19.99	4.71	3.07	63.51	0.27	0.41	0.42	2.14	0.14	2.60	3.11
FA	57.74	26.49	2.72	3.77	0.99	1.01	1.39	0.72	0.06	0.10	3.54
GWG	69.68	1.58	0.48	10.98	0.05	14.25	0.33	0.70	0.01	0.07	1.76

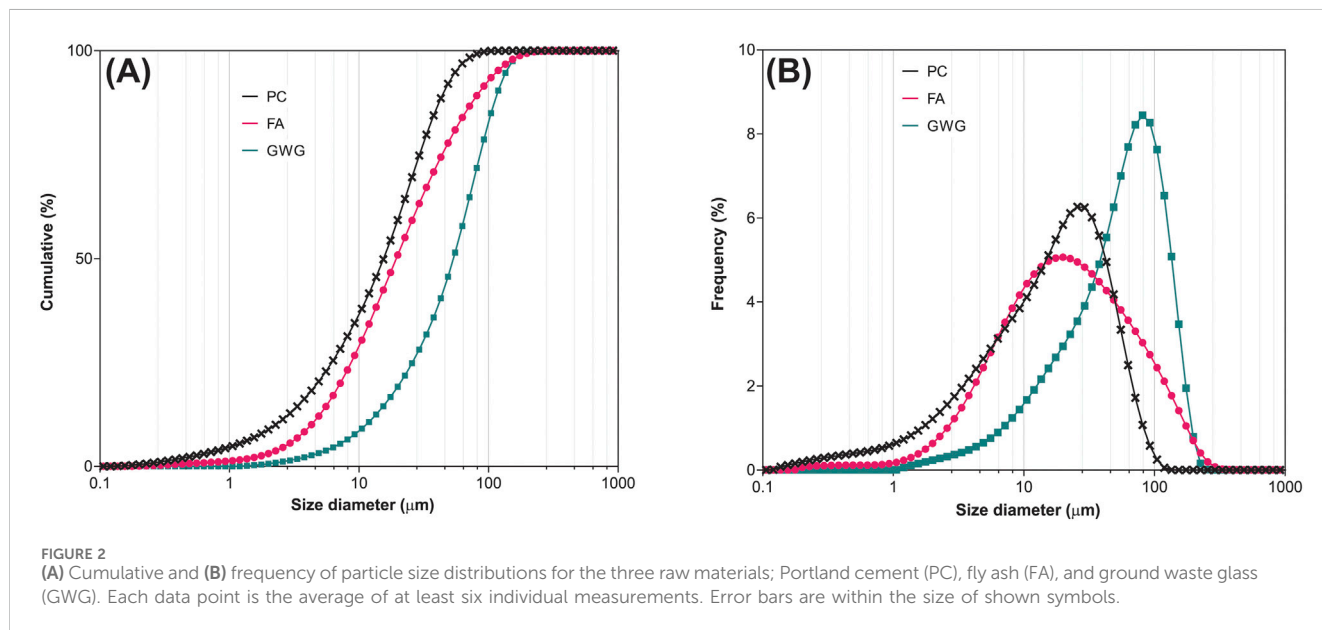


TABLE 4 Particle size distribution of PC, FA, and GWG.

Sizes (μm)	D <sub>10</sub>	D <sub>50</sub>	D <sub>90</sub>	D [4,3]
PC	2.42	16.5	48.0	21.5
FA	4.57	20.7	90.3	36.0
GWG	12.1	57.1	125	63.6

(assuming constant density throughout the system). The median particle sizes (D<sub>50</sub>) for FA and GWG were 20.7 μm and 57.1 μm respectively, both larger than PC at only 16.5 μm. Additionally, the mass-basis median values of D [4,3] are nominally 21.5 μm for PC, 36.0 μm for FA, and 63.6 μm for GWG. The particle size of the GWG is well suited to ensure pozzolanicity as a cement replacement. Bentz et al. (2012) noted that the rheological parameters, namely, yield stress and viscosity, are dependent on the particle characteristics of the materials with constant water volume fraction.

### 2.6 Rheological properties of fresh cement paste

The rheological properties of the mixtures were measured using an Anton Paar MCR rheometer fitted with 25 mm parallel plates. A similar rheological protocol was adapted from Moïni et al. (2018) to compute the values of yield stress and viscosity against shear rates.

### 2.7 Extrusion rate of mixtures

The shear rate ( $\dot{\gamma}$ ) for each of the mixtures at the nozzle tip was calculated using Equation 1:

$$\dot{\gamma} = \frac{4Q}{\pi r^3} \tag{1}$$

where Q is the volumetric flow rate, obtained by measuring mass extruded over a specified time period of 10 min and based on the density of the fresh paste mixture.

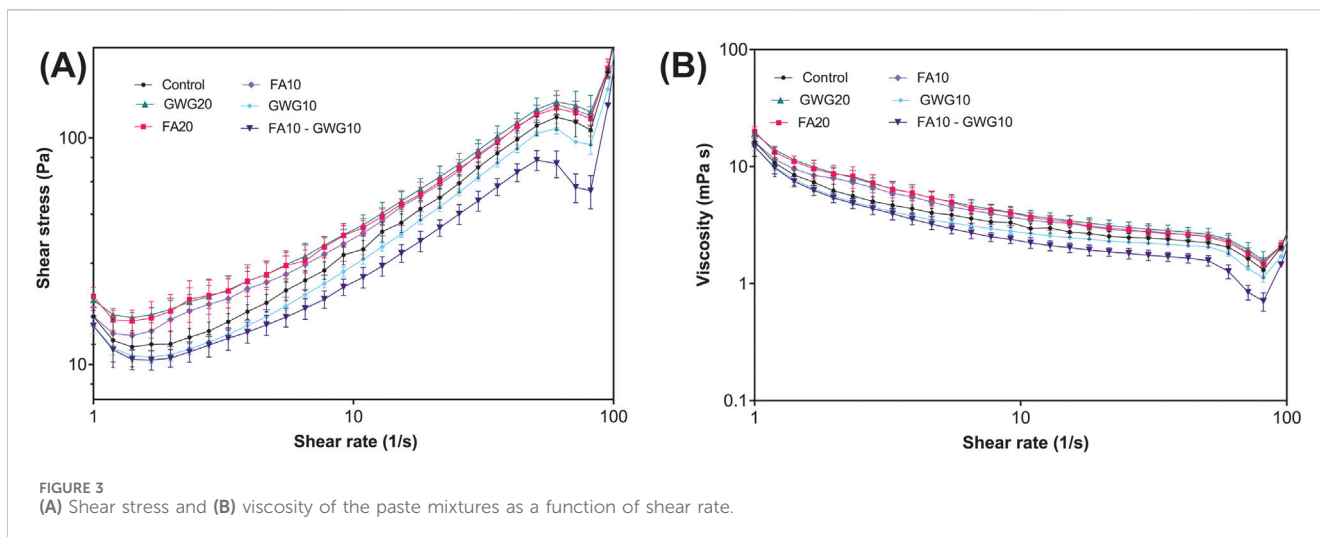
The curve data of shear stress as a function of shear rate from Figure 3 were fitted into a linear Equation 2, with ordinary least squares regression to obtain a slope (plastic viscosity) and the intercept (yield stress) according to the Bingham model:

$$\tau = \tau_0 + \eta \dot{\gamma} \tag{2}$$

where  $\tau$  is the measured shear stress at the computed shear rate  $\dot{\gamma}$ ,  $\tau_0$  is the yield stress, and  $\eta$  is the plastic viscosity.

### 2.8 Flexural strength–Modulus of rupture (MOR)

This study focuses on flexural strength due to the 3D printed unique geometries of layer-by-layer construction, resulting in a sufficient bending stress. Hence, flexural strength is crucial in assessing its structural integrity. Future work may incorporate



comprehensive strengths. The ball on three ball test was used in this study as it is more tolerant to non-flatness of the disc than other biaxial strength testing method for brittle materials applied for thin discs (Börger et al., 2002). It allowed ease of preparation and quick testing of samples. The thin circular disc specimens with an average of diameter of 55 and 8 mm in height, rested on three symmetrically spaced steel balls near its periphery. Force was applied to the center of the disc at a specified constant rate in a compression testing frame (Tinius Olsen H5KS). A fourth ball of the same size was loaded facing down the upper face of the centrally loaded disc samples. The force was applied to the center of the disk at a prescribed constant rate in a compression test machine (Tinius Olsen) until the specimens were broken. All specimens were tested at the age of 3 days (72 h) and reported data were an average of three results.

Analytical solutions were used in this approach to calculate the maximum tensile stress ( $\sigma_{max}$ ) in the center of the discs. They are given by Equations 3, 4 (Shetty et al., 1980; Börger et al., 2002):

$$\sigma_{max} = \frac{3 \cdot F \cdot (1 + \nu)}{4\pi \cdot t^2} \left[ 1 + 2 \ln \left( \frac{R_a}{R_b} \right) + \frac{1 - \nu}{1 + \nu} \left( \frac{2R_a^2 - R_b^2}{2R^2} \right) \right] \quad (3)$$

with  $R_b$  as the approximation of the contact radius of the central loading ball. For the ball on three ball test method, this was estimated by:

$$R_b = \frac{t}{3} \quad (4)$$

Where  $F$  represents the force,  $t$  the sample thickness,  $R$  the radius of the disc sample,  $R_a$  the radius of the support circle,  $R_b$  the contact radius of the loading ball, and  $\nu$  the Poisson ratio of disc material (assumed to be 0.20).

## 2.9 Statistical analysis

Statistical analysis was conducted to rigorously evaluate the significance of the results obtained. Firstly, the data were presented as the mean of triplicate measurements unless otherwise specified, ensuring the reliability and reproducibility of the findings. Subsequently, analysis of variance (ANOVA) was

employed using RStudio, a statistical software package, with a significance level of 0.05. This allowed for comprehensive comparison of multiple sample groups to determine if there were any significant differences among them. Additionally, to pinpoint specific differences between individual sample pairs, a Least Significant Difference (LSD) post-hoc test was performed. This post-hoc analysis enabled a more detailed examination of pairwise differences, ensuring a thorough understanding of the experimental outcomes.

## 3 Results and discussion

Figure 4 shows the arial view of the product for post-properties analysis.

### 3.1 Rheological properties—Yield stress and viscosity

The extruded mass and density for each mixture are summarized in Table 5 along with the volumetric flow rate and shear rate calculated with nozzle internal radius  $r$  of 0.775 mm. Values are the average of three replicates.

The rheological behavior of all the paste mixes were similar to the control mix, fitting the Bingham model and exhibiting a non-Newtonian, thixotropic fluid characteristic as expected for cement pastes. It was concluded previously by Rehman and Kim (2021) that there were no absolute range values of yield stress and plastic viscosity for printable concrete. Additionally, even with the same mix, rheological values measured with two different rheometers can differ. A single mix design is exclusive to one printer settings and may not be printable with another because of the unique setup of each printer used in their respective studies such as nozzle diameter, pump, and extrusion system. Thus, the rheological results in this study are discussed in relation to the control mix proportion.

Yield stress is the minimum strength required to initiate flow in a mixture. The inclusion of waste materials significantly influences both the yield stress and viscosity ( $p < 0.05$ ). Adding FA improves

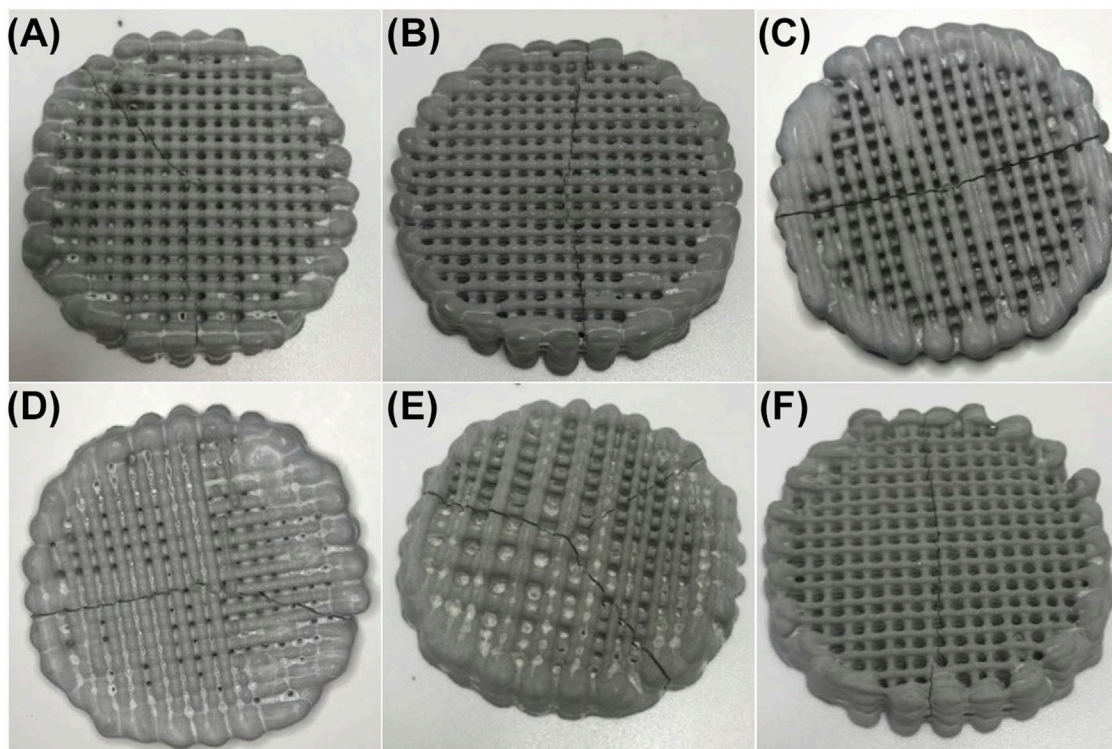


FIGURE 4 Top view of the 3D concrete material, from top left to bottom right mixture; (A) control, (B) FA10, (C) FA20, (D) GWG10, (E) GWG20, (F) FA10-GWG10.

TABLE 5 The total of extruded mass over 10 min of each blend and their corresponding paste density, measured volumetric flow rate, shear rate, and viscosity. Means that are significantly different based on the LSD analysis are labelled with different letters.

Mix	Mass extruded (g/10min)	Paste density (g/cm <sup>3</sup> )	Q (mm <sup>3</sup> /s)	Shear rate (s <sup>-1</sup> )	Viscosity (Pa s)	Yield stress (Pa)	Relative yield stress
Control	10.40	2.085	8.310	22.73	2.52 <sup>bc</sup>	9.906 <sup>b</sup>	1.000
FA10	10.00	2.075	8.057	22.04	2.89 <sup>ab</sup>	12.11 <sup>ab</sup>	1.222
FA20	8.56	1.937	7.372	20.16	3.03 <sup>a</sup>	14.54 <sup>a</sup>	1.467
GWG10	10.10	1.957	8.627	23.60	2.28 <sup>cd</sup>	9.038 <sup>bc</sup>	0.912
GWG20	9.10	2.033	7.457	20.40	0.89 <sup>a</sup>	6.304 <sup>c</sup>	0.636
FA10-GWG10	9.47	2.068	7.628	20.86	1.88 <sup>d</sup>	10.10 <sup>b</sup>	1.019

workability and reduces water demand due to the spherical shape of its particles, and lowers the surface to volume ratio—an effect known as the ball bearing effect (Bentz et al., 2012). As the proportion of FA used as cement replacement increases, there is evidence of a corresponding increase in the yield stress. Conversely, mixtures with 10% and 20% GWG show a decreasing trend in yield stress, as detailed in Table 5. The rise in yield stress with increased FA is consistent with findings by Rehman et al. (2020), suggesting that FA is beneficial in situations where the yield stress of the cement paste is initially low, in order to help maintain the shape of the printed layers. In contrast, both yield stress and viscosity decrease when a higher proportion of GWG replaces cement, indicating weaker

interparticle forces between cement and glass compared to cement with itself. This agrees with the results of Du and Tan (2014), whose study demonstrates that increasing the glass content reduces the interaction between cement and water, attributing this to the negligible water absorption and smooth surface of glass powder.

### 3.2 Comparison of MOR and work of failure (WOF)

The flexural strength (modulus of rupture) of 3D printed thin disc samples was evaluated for six different mixtures, provided in

TABLE 6 Average values of MOR of printed and cast samples. Significantly different values are labeled with different letters.

Mix	Type	MOR (MPa)
Control	Cast	18.194 <sup>a</sup>
GWG10	Cast	14.477 <sup>ab</sup>
GWG20	Cast	13.991 <sup>bc</sup>
GWG20	Print	13.448 <sup>bcd</sup>
FA20	Cast	11.940 <sup>bcd</sup>
FA10-GWG10	Cast	11.836 <sup>bcd</sup>
FA10	Cast	11.449 <sup>bcd</sup>
FA10	Print	10.200 <sup>cde</sup>
GWG10	Print	9.820 <sup>def</sup>
FA10-GWG10	Print	7.687 <sup>ef</sup>
FA20	Print	7.658 <sup>ef</sup>
Control	Print	6.163 <sup>f</sup>

Table 6 and shown in Figure 5 compared to their cast counterparts of similar disc dimensions.

Table 6 presents the average MOR values for both printed and cast specimens across the six mixtures. An ANOVA analysis was conducted to examine the interaction between different mixtures and the printing/casting methods in terms of their MOR outcomes. The analysis yielded a *p*-value of 0.00489, indicating a significant interaction effect between the mixtures and the fabrication methods. This finding suggests that the strength of the MOR is not solely determined by whether the specimen is printed or cast, but also significantly depends on the specific proportions and combinations of waste materials used in each mixture.

The highest average MOR was observed in the cast control specimens (18.2 MPa). However, the lowest MOR was found in

the printed counterparts (6.16 MPa). This suggests that using only cement (control) without waste additives may not be optimal for the printing method. Incorporating additional waste materials appears to be a more effective strategy for 3D printing. The best MOR for a printed sample was achieved with the GWG20 blend, where no significant difference was found between the cast and printed methods. This indicates that the GWG20 mixture performs equally well in both fabrication techniques.

The WOF was determined by integrating the area under the load-displacement curves for each sample and is shown in Table 7. Figure 6 depicts the WOF values for all printed samples from the different mixture designs, each replicated three times. The analysis reveals a significant difference in the WOF across all mixtures (*p* > 0.05). According to the data in Table 7, there was no interaction effect between the two types of waste materials on the WOF, i.e., both types were found to perform comparably to the control. Specifically, the FA10 mixture achieved the highest WOF value, while the GWG20 mixture recorded the lowest.

The ball-on-three ball test is a quick and easy to use method to study the biaxial strength of particularly new brittle materials (Danzer et al., 2007). Hence, it is well suited for small specimens used in this study. Overall, the 3D printed specimens showed lower average strength compared to their cast counterparts. This is associated with the inherent nature of porous regions when cement was printed, unlike that of solid blocks achieved when specimens were cast.

For cast cement, the control mixture achieved the highest strength compared to all mixtures with waste replacements, likely due to the coarser particle size of FA and GWG compared to PC (Chindaprasirt et al., 2005; Tamanna and Tuladhar, 2020). The cast control mixture recorded an average strength of 18.2 MPa. The FA10 and FA20 mixtures achieved 63% and 66% of the control mixture’s strength, respectively. In terms of flexural strength, cast mixtures with waste glass showed a decrease as the percentage of GWG replacement increased; GWG10 and GWG20 achieved 80%

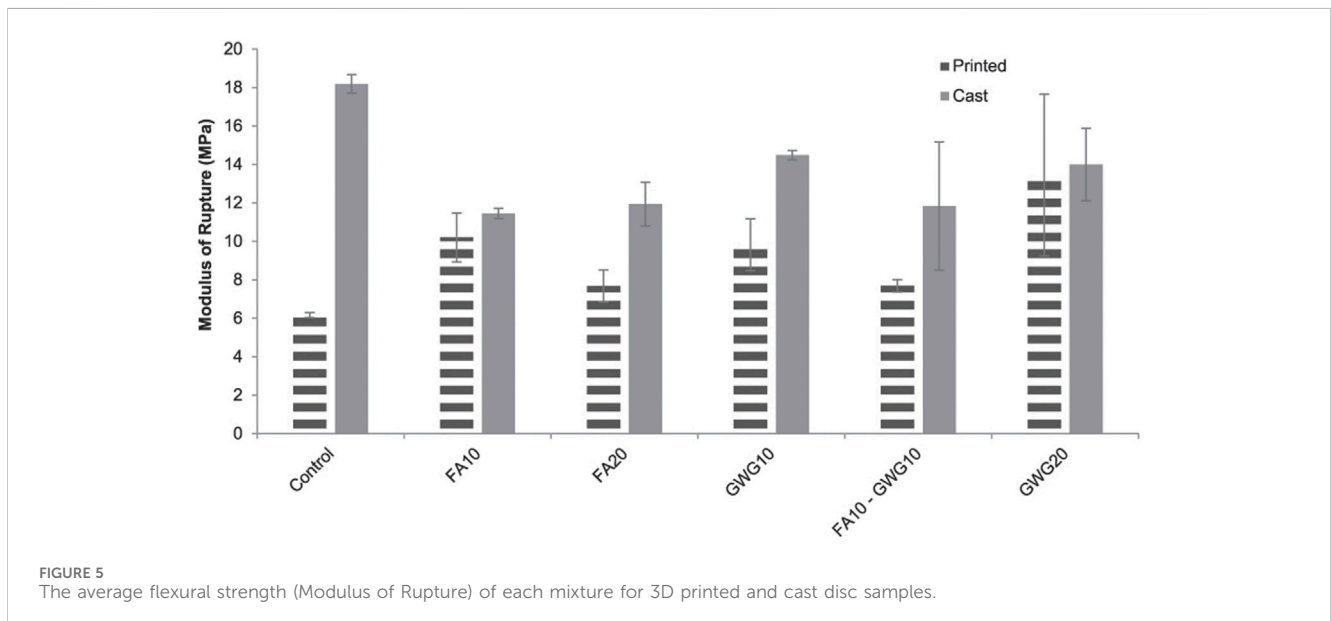


TABLE 7 Work of Failure (WOF) of printed samples. Means that were significantly different based on the LSD analysis are labelled with different letters.

Mix	WOF (N cm)
FA10	2.508 <sup>a</sup>
GWG10	2.451 <sup>a</sup>
FA20	2.061 <sup>ab</sup>
Control	1.810 <sup>ab</sup>
FA10-GWG10	1.770 <sup>b</sup>
GWG20	1.654 <sup>b</sup>

and 77% of the control strength, respectively. Mixtures with waste glass exhibited slightly higher flexural strength than those with FA. This can be attributed to the high SiO<sub>2</sub> content in GWG (70% SiO<sub>2</sub>) and its angular structure, which provides a larger surface area compared to the spherical FA particles. GWG chemically reacts with calcium hydroxide in the cement to form calcium silicate hydrate (CSH), the primary hydration product in hardened cement paste (Turgut and Yahlizade, 2009). The formation of CSH contributes to higher strength and a pore-blocking effect when GWG is used as a pozzolan replacement (Turgut and Yahlizade, 2009).

The inclusion of different types of waste materials significantly influenced the flexural strength of the 3D printed disc samples. The reference control mixture experienced the most substantial reduction in average flexural strength when comparing cast and printed forms, with a 66% decrease. In contrast, mixtures containing waste materials showed a smaller reduction in strength in the following descending order: FA20 and FA10-GWG10 both at 35%, GWG10 at 32%, FA10 at 11%, and GWG20 at only 4%.

The flexural strength of printed samples with increasing FA content showed a decline: samples with 10% FA ranged from 8 to 11 MPa, and those with 20% FA from 7 to 8 MPa. This reduction in strength could be attributed to a delay in the hydration process caused by the ashes, as noted by Bui Viet et al. (2020), suggesting that a longer-term study on strength development might be necessary.

When assessing the flexural strength of 3D printed versus cast samples, several factors must be considered: (1) material composition, (2) printing parameters, (3) curing conditions, and (4) testing methods. In this paper, the material, curing, and testing conditions were standardized across both printing and casting methods. Interestingly, all 3D printed specimens that incorporated waste materials exhibited higher flexural strengths than the control mixture, which averaged 6 MPa. The highest performing was GWG20, with strengths ranging from 10 to 18 MPa, followed by FA10 (8–11 MPa), GWG10 (8–10 MPa), FA20 (7–8 MPa), and FA10-GWG10 (7–8 MPa). This trend contrasts with that of the cast specimens, where the control mixture achieved the highest strength. The printed structures displayed enhanced fracture resistance or toughness, attributed to the specific pitch angle of the filaments during printing, which effectively distributed stress along the filaments and enhanced their ability to resist fractures (Moini et al., 2018).

### 3.3 Load–Displacement curve

The load-displacement responses of printed and cast control and GWG20 specimens were analyzed using the ball-on-three ball test method and are presented in Figure 7. This figure compares the control mixture to the GWG20 mixture, which exhibits the highest MOR. The slope of the ascending

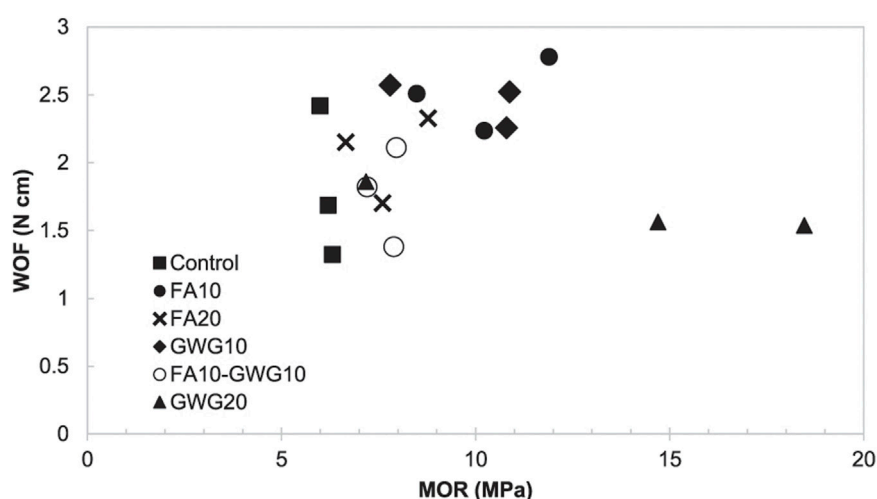


FIGURE 6 WOF vs MOR of printed specimens of Bouligand architecture.

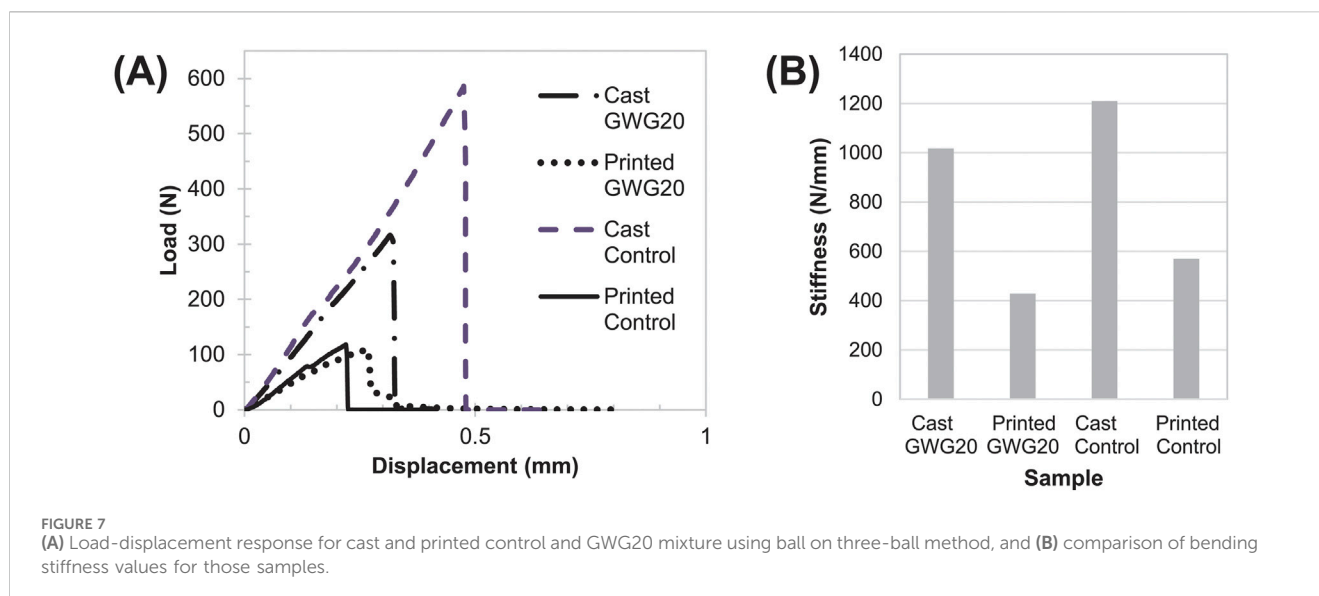


FIGURE 7 (A) Load-displacement response for cast and printed control and GWG20 mixture using ball on three-ball method, and (B) comparison of bending stiffness values for those samples.

section of the load-displacement graph represents the bending stiffness under impact-induced bending (Karahan and Yildirim, 2015). A comparison of these stiffness values is also featured in Figure 6, alongside the load-displacement curves.

The cast control sample demonstrated the highest stiffness, followed by the cast GWG20. Figure 6 shows that the deflection at maximum load for the printed GWG20 is greater than that of its cast counterpart. Additionally, the curves for both the cast control and GWG20 mixtures are steeper compared to those of the printed specimens, indicating more brittle properties.

The printed specimens, utilizing the Bouligand architecture, show an ability to mitigate catastrophic failure—a feature not observed in the cast specimens. The printed specimens display a more gradual and distributed damage pattern throughout the layers, preventing the drastic drops seen in the cast curves. This illustrates the advantage of the 3D printing method in enhancing structural integrity and resilience against catastrophic failure.

## 4 Conclusion

This study investigates the use of FA and GWG as sustainable alternatives to PC in 3D concrete printing, focusing on their effects on the rheological and mechanical properties of the printed structures. Experimental results indicate that FA increases yield stress, aiding in shape retention under stress, while GWG decreases yield stress, promoting smoother extrusion during printing. The cast concrete mixtures achieved higher MOR values, with the highest at 18.2 MPa, compared to their printed counterparts, which showed reduced strength. Notably, the GWG20 mixture exhibited the highest MOR among printed samples at 13.4 MPa, suggesting that high waste content can potentially match or surpass the performance of traditional materials in specific conditions.

The incorporation of GWG and FA not only reduces dependence on virgin cement but also enhances the mechanical properties of the concrete, achieving comparable or superior flexural strength and fracture resistance, particularly when utilizing complex

geometrical structures like the Bouligand architecture. This architecture effectively distributes stress and mitigates fracture risk, enhancing material toughness. These findings highlight the potential for the construction industry to reduce its carbon footprint and leverage 3D printing for more sustainable and efficient building practices. However, the observed performance variability between printed and cast forms necessitates further research into long-term strength development, the effects of porosity and microstructure, and optimized material combinations and printing conditions. Establishing standardized comparison frameworks for 3D printing mixes will aid in maximizing environmental and mechanical benefits, advancing the industry's ability to meet modern demands sustainably.

## Data availability statement

The original contributions presented in the study are included in the article/Supplementary Material, further inquiries can be directed to the corresponding author.

## Author contributions

PS: Data curation, Formal Analysis, Investigation, Methodology, Software, Validation, Visualization, Writing—original draft. YC: Methodology, Validation, Visualization, Writing—review and editing. GF-W: Supervision, Visualization, Writing—review and editing. ES: Visualization, Writing—review and editing. AA: Conceptualization, Funding acquisition, Methodology, Project administration, Resources, Supervision, Writing—review and editing.

## Funding

The author(s) declare that no financial support was received for the research, authorship, and/or publication of this article.

## Acknowledgments

The authors would like to extend their gratitude to Delta Electricity for supplying the fly ash, and IQ Renew for supplying the ground glass. The authors would also like to thank Associate Professor Daniel Dias-da-Costa for initial contributions and valuable discussions during the development of this work, and Assistant Professor Reza Moini for his input on the manuscript.

## Conflict of interest

The authors declare that the research was conducted in the absence of any commercial or financial relationships that could be construed as a potential conflict of interest.

## References

- Aïtcin, P. (2016). "Supplementary cementitious materials and blended cements," in *Science and technology of concrete admixtures* (Cambridge, United Kingdom: Woodhead publishing), 53–73. doi:10.1016/B978-0-08-100693-1.00004-7
- Atradius (2023). Construction industry trends 2023. Available at: <https://atradius.com.hk/en/publications/construction-industry-trends-global-overview-2023.html> (Accessed May 5, 2024).
- Batikha, M., Jotangia, R., Baaj, M. Y., and Mousleh, I. (2022). 3D concrete printing for sustainable and economical construction: a comparative study. *Automation Constr.* 134, 104087. doi:10.1016/j.autcon.2021.104087
- Benhelal, E., Zahedi, G., Shamsaei, E., and Bahadori, A. (2013). Global strategies and potentials to curb CO<sub>2</sub> emissions in cement industry. *J. Clean. Prod.* 51, 142–161. doi:10.1016/j.jclepro.2012.10.049
- Bentz, D. P., Ferraris, C. F., Galler, M. A., Hansen, A. S., and Guynn, J. M. (2012). Influence of particle size distributions on yield stress and viscosity of cement–fly ash pastes. *Cem. Concr. Res.* 42, 404–409. doi:10.1016/j.cemconres.2011.11.006
- Bignozzi, M., Sacconi, A., Barbieri, L., and Lancellotti, I. (2015). Glass waste as supplementary cementing materials: the effects of glass chemical composition. *Cem. Concr. Compos.* 55, 45–52. doi:10.1016/j.cemconcomp.2014.07.020
- Börger, A., Supancic, P., and Danzer, R. (2002). The ball on three balls test for strength testing of brittle discs: stress distribution in the disc. *J. Eur. Ceram. Soc.* 22, 1425–1436. doi:10.1016/S0955-2219(01)00458-7
- Bui Viet, D. B., Chan, W.-P., Phua, Z.-H., Ebrahimi, A., Abbas, A., and Lisak, G. (2020). The use of fly ashes from waste-to-energy processes as mineral CO<sub>2</sub> sequestrators and supplementary cementitious materials. *J. Hazard. Mater.* 398, 122906. doi:10.1016/j.jhazmat.2020.122906
- Chindaprasirt, P., Jaturapitakkul, C., and Sinsiri, T. (2005). Effect of fly ash fineness on compressive strength and pore size of blended cement paste. *Cem. Concr. Compos.* 27, 425–428. doi:10.1016/j.cemconcomp.2004.07.003
- Danzer, R., Harrer, W., Supancic, P., Lube, T., Wang, Z., and Börger, A. (2007). The ball on three balls test—strength and failure analysis of different materials. *J. Eur. Ceram. Soc.* 27, 1481–1485. doi:10.1016/j.jeurceramsoc.2006.05.034
- Dey, D., Srinivas, D., Panda, B., Suraneni, P., and Sitharam, T. (2022). Use of industrial waste materials for 3D printing of sustainable concrete: a review. *J. Clean. Prod.* 340, 130749. doi:10.1016/j.jclepro.2022.130749
- Du, H., and Tan, K. H. (2014). Waste glass powder as cement replacement in concrete. *J. Adv. Concr. Technol.* 12, 468–477. doi:10.3151/jact.12.468
- Ebrahimi, A., Saffari, M., Milani, D., Montoya, A., Valix, M., and Abbas, A. (2017). Sustainable transformation of fly ash industrial waste into a construction cement blend via CO<sub>2</sub> carbonation. *J. Clean. Prod.* 156, 660–669. doi:10.1016/j.jclepro.2017.04.037
- Karahan, M., and Yildirim, K. (2015). "Low velocity impact behaviour of Aramid and UHMWPE composites," in *Fibres textiles in eastern europe*, 97–105.
- Liu, J., Li, S., Fox, K., and Tran, P. (2022). 3D concrete printing of bioinspired Bouligand structure: a study on impact resistance. *J. Addit. Manuf.* 50, 102544. doi:10.1016/j.addma.2021.102544
- Moini, M., Olek, J., Youngblood, J. P., Magee, B., and Zavattieri, P. D. (2018). Additive manufacturing and performance of architected cement-based materials. *Adv. Mater.* 30, 1802123. doi:10.1002/adma.201802123
- Muthukrishnan, S., Kua, H. W., Yu, L. N., and Chung, J. K. (2020). Fresh properties of cementitious materials containing rice husk ash for construction 3D printing. *J. Mater. Civ. Eng.* 32, 04020195. doi:10.1061/(asce)mt.1943-5533.0003230
- Nodehi, M., and Taghvaei, V. M. (2021). Sustainable concrete for circular economy: a review on use of waste glass. *Glass Struct. & Eng.* 7, 3–22. doi:10.1007/s40940-021-00155-9
- Panda, B., Lim, J. H., and Tan, M. J. (2019). Mechanical properties and deformation behaviour of early age concrete in the context of digital construction. *Compos. Part B Eng.* 165, 563–571. doi:10.1016/j.compositesb.2019.02.040
- Qian, H., Hua, S., Gao, Y., Qian, L., and Ren, X. (2021). Synergistic effect of EVA copolymer and sodium desulfurization ash on the printing performance of high volume blast furnace slag mixtures. *Addit. Manuf.* 46, 102183. doi:10.1016/j.addma.2021.102183
- Rehman, A. U., and Kim, J.-H. (2021). 3D concrete printing: a systematic review of rheology, mix designs, mechanical, microstructural, and durability characteristics. *Materials* 14, 3800. doi:10.3390/ma14143800
- Rehman, A. U., Lee, S.-M., and Kim, J.-H. (2020). Use of municipal solid waste incineration ash in 3D printable concrete. *Process Saf. & Environ. Prot.* 142, 219–228. doi:10.1016/j.psep.2020.06.018
- Reiter, L., Wangler, T., Roussel, N., and Flatt, R. J. (2018). The role of early age structural build-up in digital fabrication with concrete. *Cem. Concr. Res.* 112, 86–95. doi:10.1016/j.cemconres.2018.05.011
- Roussel, N. (2018). Rheological requirements for printable concretes. *Cem. Concr. Res.* 112, 76–85. doi:10.1016/j.cemconres.2018.04.005
- Rubio, M., Sonebi, M., and Amziane, S. (2017). Fresh and rheological properties of 3D printing bio-cement-based materials. *Acad. J. Civ. Eng.* 35, 283–290. doi:10.26168/icbbm2017.43
- Şahin, O., İlcan, H., Ateşli, A. T., Kul, A., Yıldırım, G., and Şahmaran, M. (2021). Construction and demolition waste-based geopolymers suited for use in 3-dimensional additive manufacturing. *Cem. Concr. Compos.* 121, 104088. doi:10.1016/j.cemconcomp.2021.104088
- Shetty, D. K., Rosenfield, A. R., Mcguire, P., Bansal, G. K., and Duckworth, W. H. (1980). Biaxial flexure tests for ceramics. *Am. Ceram. Soc. Bull.* 59, 1193–1197.
- Singh, A., Wang, Y., Zhou, Y., Sun, J., Xu, X., Li, Y., et al. (2023). Utilization of antimony tailings in fiber-reinforced 3D printed concrete: a sustainable approach for construction materials. *J. Constr. Build. Mater.* 408, 133689. doi:10.1016/j.conbuildmat.2023.133689
- Sun, J., Aslani, F., Wei, J., and Wang, X. (2021a). Electromagnetic absorption of copper fiber oriented composite using 3D printing. *J. Constr. Build. Mater.* 300, 124026. doi:10.1016/j.conbuildmat.2021.124026
- Sun, J., Huang, Y., Aslani, F., and Ma, G. (2020). Electromagnetic wave absorbing performance of 3D printed wave-shape copper solid cementitious element. *J. Cem. Concr. Compos.* 114, 103789. doi:10.1016/j.cemconcomp.2020.103789
- Sun, J., Tang, W., Wang, Y., Yao, X., Huang, B., Saafi, M., et al. (2023). Electromagnetic and mechanical performance of 3D printed wave-shaped copper solid superstructures. *J. J. Mater. Res. Technol.* 27, 6936–6946. doi:10.1016/j.jmrt.2023.11.116
- Sun, J., Wang, Y., Liu, S., Dehghani, A., Xiang, X., Wei, J., et al. (2021b). Mechanical, chemical and hydrothermal activation for waste glass reinforced cement. *J. Constr. Build. Mater.* 301, 124361. doi:10.1016/j.conbuildmat.2021.124361
- Tagnit-Hamou, A., Soliman, N., and Omran, A. (2016). "Green ultra-high-performance glass concrete," in International interactive symposium on ultra-high performance concrete, Des Moines, Iowa, (July 18–20, 2016) (Iowa State University Digital Press). doi:10.21838/uhpc.2016.35

## Publisher's note

All claims expressed in this article are solely those of the authors and do not necessarily represent those of their affiliated organizations, or those of the publisher, the editors and the reviewers. Any product that may be evaluated in this article, or claim that may be made by its manufacturer, is not guaranteed or endorsed by the publisher.

## Supplementary material

The Supplementary Material for this article can be found online at: <https://www.frontiersin.org/articles/10.3389/fbuil.2024.1430174/full#supplementary-material>

- Tamanna, N., and Tuladhar, R. (2020). Sustainable use of recycled glass powder as cement replacement in concrete. *Open Waste Manag. J.* 13, 1–13. doi:10.2174/1874347102013010001
- Turgut, P., and Yahlizade, E. (2009). Research into concrete blocks with waste glass. *Int. J. Civ. Environ. Eng.* 1, 203–209.
- Xia, M., Nematollahi, B., and Sanjayan, J. (2019). Printability, accuracy and strength of geopolymer made using powder-based 3D printing for construction applications. *Automation Constr.* 101, 179–189. doi:10.1016/j.autcon.2019.01.013
- Yao, X., Lyu, X., Sun, J., Wang, B., Wang, Y., Yang, M., et al. (2023). AI-based performance prediction for 3D-printed concrete considering anisotropy and steam curing condition. *J. Constr. Build. Mater.* 375, 130898. doi:10.1016/j.conbuildmat.2023.130898
- Yin, W., Li, X., Sun, T., Chen, Y., Xu, F., Yan, G., et al. (2021). Utilization of waste glass powder as partial replacement of cement for the cementitious grouts with superplasticizer and viscosity modifying agent binary mixtures: rheological and mechanical performances. *Constr. Build. Mater.* 286, 122953. doi:10.1016/j.conbuildmat.2021.122953
- Zhu, B., Wang, Y., Sun, J., Wei, Y., Ye, H., Zhao, H., et al. (2023). An experimental study on the influence of waste rubber particles on the compressive, flexural and impact properties of 3D printable sustainable cementitious composites. *J. Case Stud. Constr. Mater.* 19, e02607. doi:10.1016/j.cscm.2023.e02607